Supporting Information for

Imaging Electrochemically Regulated Water-air Nanointerfaces with Single-molecule Fluorescence

Guopeng Li‡[1234], Lisi Wen‡[234], Runfeng Sun[234] and Rui Hao*[234]

1 Department of chemistry and chemical engineering, Harbin Institute of Technology, 150006 Harbin, China

2 Department of Chemistry, Southern University of Science and Technology, 518055 Shenzhen, China

3 Research Center for Chemical Biology and Omics Analysis, Southern University of Science and Technology, 518055 Shenzhen, China

4 Shenzhen Key Laboratory of Functional Proteomics, Southern University of Science and Technology, 518055 Shenzhen, China

* Email: haor@sustech.edu.cn

‡ These authors contributed equally.

Table of Contents

1. Experimental Section

Chemicals: All chemicals were directly used as received from the manufacturer and Include sulfo-cyanine5.5 (Cy5.5, 100%, Sigma-Aldrich), cyanine 5-N-hydroxysuccinimide (+Cy5, 100%, Sigma-Aldrich), sodium dodecyl sulfate (SDS, Molecular Biology, Sangon Biotech), cetyl trimethyl ammonium bromide (CTAB, Molecular Biology, Sigma-Aldrich), phosphate buffered saline (PBS, 1×, pH 7, Macklin), acetic acid sodium acetate buffer solution (CH_3COOH-CH_3COONa buffer, 1 mol / L, pH 4, Macklin), 2-amino-2-methyl-1-propanol buffer (AMP buffer, 0.5 M, pH 10, Macklin), standard solutions of sulfuric acid (H_2SO_4, pH 1, 0.5 M, Macklin), standard solutions of potassium hydroxide (KOH, pH 14, 1M, Macklin), 1H,1H,2H,2H-Perfluorodecanethiol ($CF_3(CF_2)_7CH_2CH_2SH$, 97%, Macklin), 1H,1H,2H,2H-heptadecafluorodecyl ($C_{13}H_{13}F_{17}O_3Si$, 98%, Macklin), ethanol (CH_3CH_2OH, ≥99.8%, Aladdin), deionized water (DI water, Chemical Technology (Shenzhen)). Silicon chips with a freestanding silicon nitride window (TE100D, thickness of silicon nitride film: 200 nm, window size: 1 × 1 mm) were purchased from Suzhou in-Situ Chips Technology Co., Ltd.

Instruments: A dual-focused ion beam (FIB; Helios 600i, FEI, America) with a scanning electron microscope (SEM) was used to fabricate the nano-ring electrode arrays. An electron beam evaporation system (TF500, HHV, Britain) was used to evaporate gold (Au) and platinum (Pt) layers on the silicon nitride film window. A helium ion microscope (HIM; ORION NanoFab, Zeiss, America) was used to characterize the detailed morphology of nano-ring electrodes. An Atomic Force Microscope (AFM, MFP-3D stand-alone, Oxford, England) was used to characterize the morphology of nanodroplets. A microscope (ECLIPSE Ti2-E, Nikon, Japan) with an oil immersion objective (CFI Apochromat TIRF 60XC, Nikon; numerical aperture [NA]: 1.49) with an external 1.5 × magnification on the microscope, white light source (Nikon), 640 nm laser (GATACA SYSTEMS, Vortran, America) and corresponding laser longpass set (TRF 49914 - ET - 640 – 647 nm, Nikon, Japan), and high-speed and high-sensitivity scientific complementary metal-oxide semiconductor (sCMOS;

Kinetix, Teledyne Photometrics, China) was used for operando optical imaging of the fluorescence response. The voltage was generated by an electrochemical workstation (Vertex.One.EIS, Ivium, Germany) and applied across the working electrode (nano-ring electrode) with respect to the Ag quasi-reference counter electrode.

Fabrication of nano-ring electrode arrays: As shown in Figure S31, a nanoring electrode array was prepared in three steps. Initially, a 50 nm Au or Pt layer was evaporated on the front of a Silicon chip (The front is a silicon nitride film layer, the back is a silicon carrier) employing electron beam evaporation equipment (HHV, TF500) to ensure good conductivity of electrodes and high-precision FIB processing conditions. Subsequently, the self-assembled monolayer (SAM) of 1H,1H,2H,2H-Perfluorodecanethiol (C10H5F17S) was modified on the surface of Au or Pt layer to make its surface hydrophobic and prevent the solution from leaking out of the nanopore. Specific modifications will be detailed in the next section. Finally, the silicon chip was inverted so that its backside was facing up, and an area of approximately 25 × 25 μm was selected in the back side of the silicon nitride film window and the nanopore array was milled using a dual-beam FIB (FEI, Helios 600i) at an ion-beam current of 80 pA with the aid of the built-in scanning electron microscope for visual reference. The silicon nitride film window with a conductive layer (Pt or Au) forms perforations when irradiated with the ion beam. The final nanopore array consisted of four 1 × 5 nanopore arrays of 200, 240, 280, and 320 nm in diameter with a spacing of 5 μm, with each 1 × 5 array horizontally aligned with a spacing of 5 μm. In this way, a nano-ring electrode array is formed. Alternatively, uniform 5 × 4 uniform Au nanopore electrode arrays were prepared using the same method.

Conductive layer modification: Conductive layer modification was mainly performed using a self-assembled monolayer (SAM). Silicon nitride film windows with a conductive layer (Pt or Au) were ultraviolet (UV)-irradiated for 30 min to induce hydroxylation at the conductive layer surface. Each pretreated chip was then immersed in a solution of $CF_3(CF_2)_7CH_2CH_2SH$ in ethanol (95%) for 12 hours. Such that a monolayer containing fluoroalkyl groups was produced on the conductive layer surface. The fluoroalkyl groups decreased the surface energy, yielding a hydrophobic surface.

Construction of nanodroplet electrochemical cell: A 100 μm-thick coverslip was used as a support substrate to carry the nanodroplet electrochemical cell. In addition, another important function of this thin coverslip is to be coupled to the optical microscope with a high NA objective (short working distance (200 μm)), thus ensuring high optical imaging resolution. The construction of nanodroplet electrochemical cells is shown in Figure S32. First, double-sided conductive nonwoven tape with 3-mm-diameter perforations was glued to the coverslip surface. Second, the front side of the silicon chip prepared with nano-ring electrode arrays adhered to the conductive nonwoven tape, wherein the silicon nitride film window was in the perforated region of the conductive nonwoven tape. Due to the Au layer on the front of the silicon chip, the electrical connection between the conductive non-woven tape and the nano-ring electrode array is realized. Here, the conductive non-woven tape not only serves as an electrical connection but also anchors the silicon chip to ensure its structural stability during subsequent electrochemical testing. Moreover, the thickness of the conductive non-woven tape used in this structure is 30 μm, which is also to meet the requirements of high-resolution optical imaging. Third, the fluorophore solution is added to the recessed area on the back of the silicon chip. The solution penetrates the nanopore and contacts with the Au layer on the front of the silicon chip to achieve electrical connection. At the same time, nano-droplets are formed on the Au film side (the solution is blocked by the hydrophobic SAM and does not leak) and the water-air interface is formed at the position of the nanopore on the front of the silicon chip. Finally, the wire from the conductive nonwoven tape is connected to the working electrode of the electrochemical workstation, and the counter and reference electrodes of the electrochemical workstation are connected with a silver wire to be inserted into the exposed liquid. In this way, a nanodroplet electrochemical cell is formed in which the working electrode is an Au nano-ring electrode array and the quasi-reference counter electrode is a silver wire. Note that the size of the nanodroplets in this structure as well as the size of the water-air interface can be controlled by adjusting the size of the nanopore.

Optical imaging setup: As shown in Figure S33, the laser beam is incident at a 30°

angle and focused on the nanodroplet surface of the silicon chip, exciting fluorescent molecules in the nanodroplets to emit fluorescence and track the electrochemical response of different fluorescent molecules under different conditions. Due to limited penetration depth, incident light at 30 ° can weaken background fluorescence to some extent, thereby improving imaging resolution. The reason for not continuing to increase the incident angle is that higher incident angles make it difficult to effectively excite fluorophore. The Kinetic camera used has a temporal resolution of 50 ms and a corresponding frame rate of 20 fps. In addition, all Au nano-ring electrode arrays were first applied with a voltage of -0.2 V and then switched to 0.2 V, unless otherwise stated.

Image analysis: The image information of the electrochemical response of fluorescent molecules was processed using Image J software. In addition, Image J software was used to extract the fluorescence intensity signal during the electrochemical response of fluorescent molecules, and then Matlab self-programming code was used to extract peak height, peak width, and frequency information from the fluorescence intensity signal.

2. Supplementary Figures and Discussions

Figure S1. Calibration of quasi reference electrode (QRE)

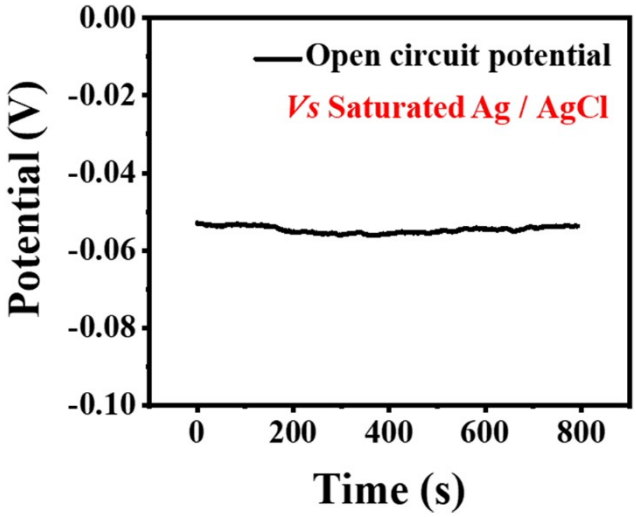

Figure S1. Calibration of QRE

As shown in Figure S1, the open-circuit potential was measured in AMP buffer with the used Ag electrode as the working electrode, and a standard saturated Ag / AgCl electrode as the reference electrode. The measurement result is -0.053 V. After calibration, the electrode potential of Ag is 0.199 V - 0.053 V = 0.146 V (vs standard hydrogen electrode (SHE)). When the potential applied to the Au nanoring electrode is -0.2 V (vs Ag), the potential is 0.146 V – 0.2 V = -0.054 V (vs SHE). When the potential applied to the Au nanoring electrode is 0.2 V (vs Ag), the potential applied to the Au nanoring electrode is 0.146 V + 0.2 V = 0.346 V (vs SHE), which is smaller than the PZC of gold. So, at 0.2 V, the charge carried on the Au nanoring electrode is negative.

Figure S2. HIM characterization result of a 5 × 4 nanopore array

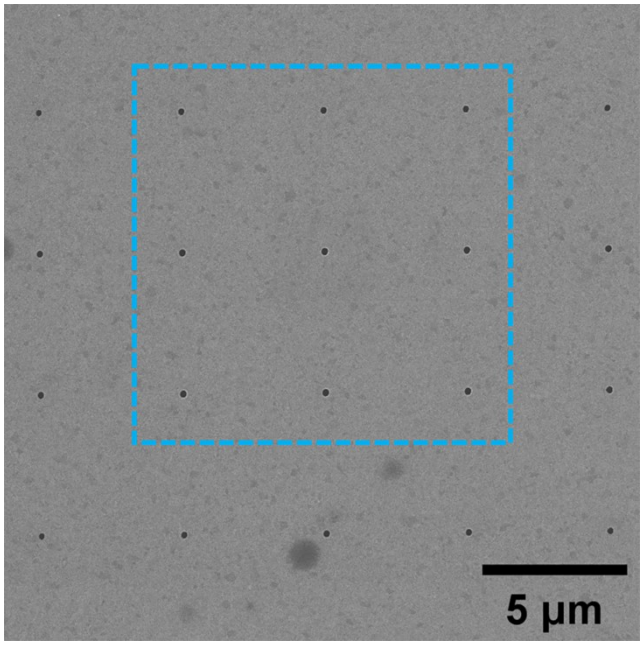

Figure S2. HIM characterization results of a uniform 5 × 4 nanopore array. The 3 × 3 nanopore array labeled by the blue box is the array shown in Figure 1B.

Figure S3. AFM measure method for characterizing curvature of nanointerfaces

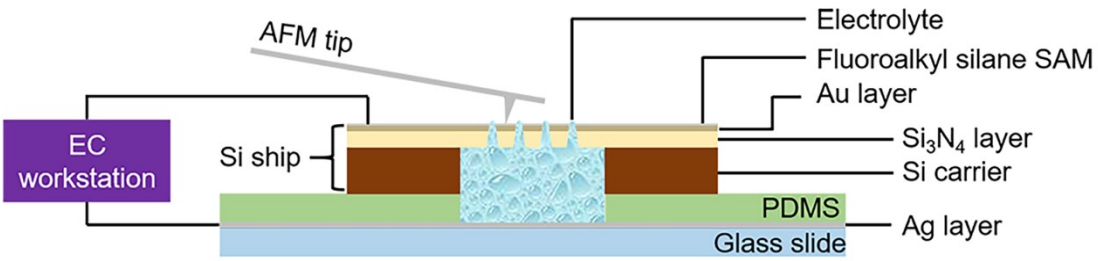

Figure S3. Structure of AFM measure method for characterizing curvature of nanointerfaces.

Figure S4. AFM characterization of nanointerfaces curvature under different conditions

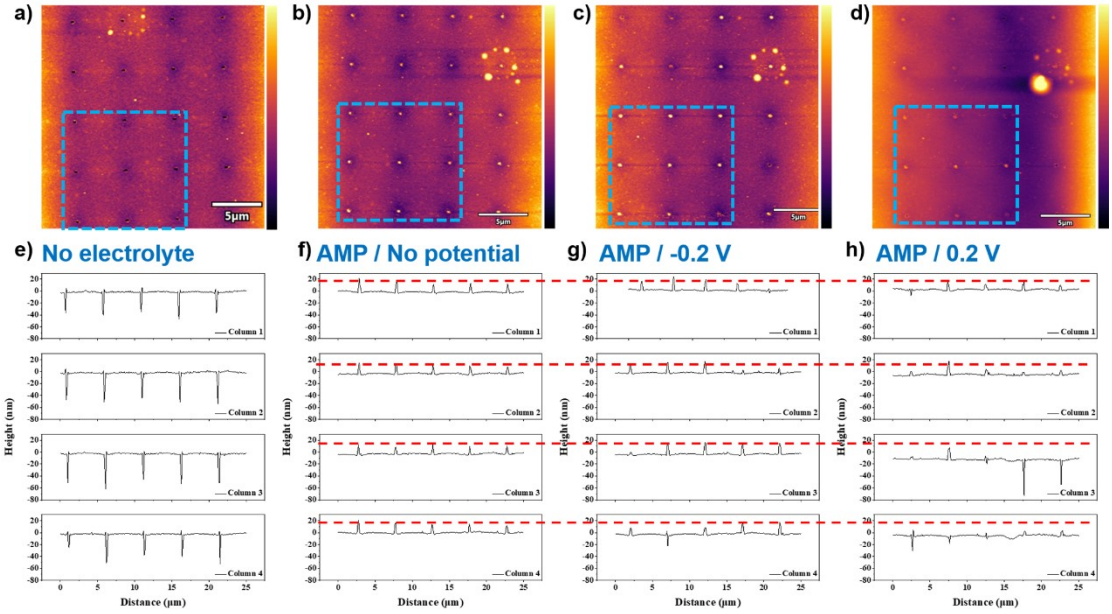

Figure S4. Detailed AFM characterization of nanointerfaces curvature with (a) no electrolyte, and AMP electrolyte at (b) no potential, (c) -0.2 V, and (d) 0.2 V. The scale bar is 5 μm. Detailed height for AFM characterization with (e) no electrolyte, and AMP electrolyte at (f) no potential, (g) -0.2 V, and (h) 0.2 V. The 3 × 3 array labeled by blue boxes are the results presented in Figure 1E-1H, respectively.

AFM tip modification

To characterize nanodroplets using AFM, it is first necessary to ensure that the AFM tip has good hydrophobicity to prevent the tip from immersing into the nanodroplets and failing to do an accurate characterization. The specific AFM tip modification method is as follows:

The modification of the AFM tip mainly uses fluoroalkyl groups ($C_{13}H_{13}F_{17}O_3Si$) to form a self-assembled monolayer (SAM) on the surface of the tip. First, AFM tips were ultraviolet (UV)-irradiated for 30 min to induce hydroxylation at the tip surface. Each pretreated chip was then immersed in an ethanol atmosphere of 5% $C_{13}H_{13}F_{17}O_3Si$ for 72 h, such that a monolayer was established on the AFM tips surface. The fluoroalkyl groups decreased the surface energy, yielding a hydrophobic surface.

Characterization of nanodroplets

First, a clean slide was prepared, and the surface was coated with an Ag layer of about 200 nm thickness using an electron beam vapor deposition system to facilitate the application of potential to the Au nanopore electrode array. Second, prepare a 100nm thickness PDMS with a 2mm diameter perforation and adhere to the slide. The perforation serves as a space for storing the electrolyte on the one hand and exposes the Ag layer for electrical connection on the other. Thirdly, The Si chip with Au nanopore electrode array was inverted and placed on PDMS. The Si chip is closely attached to the PDMS to prevent the leakage of the electrolyte, the electrolyte will enter the nanopore and form nanodroplets. Finally, the device was characterized under AFM.

Figure S5. Fluorophores structure formula

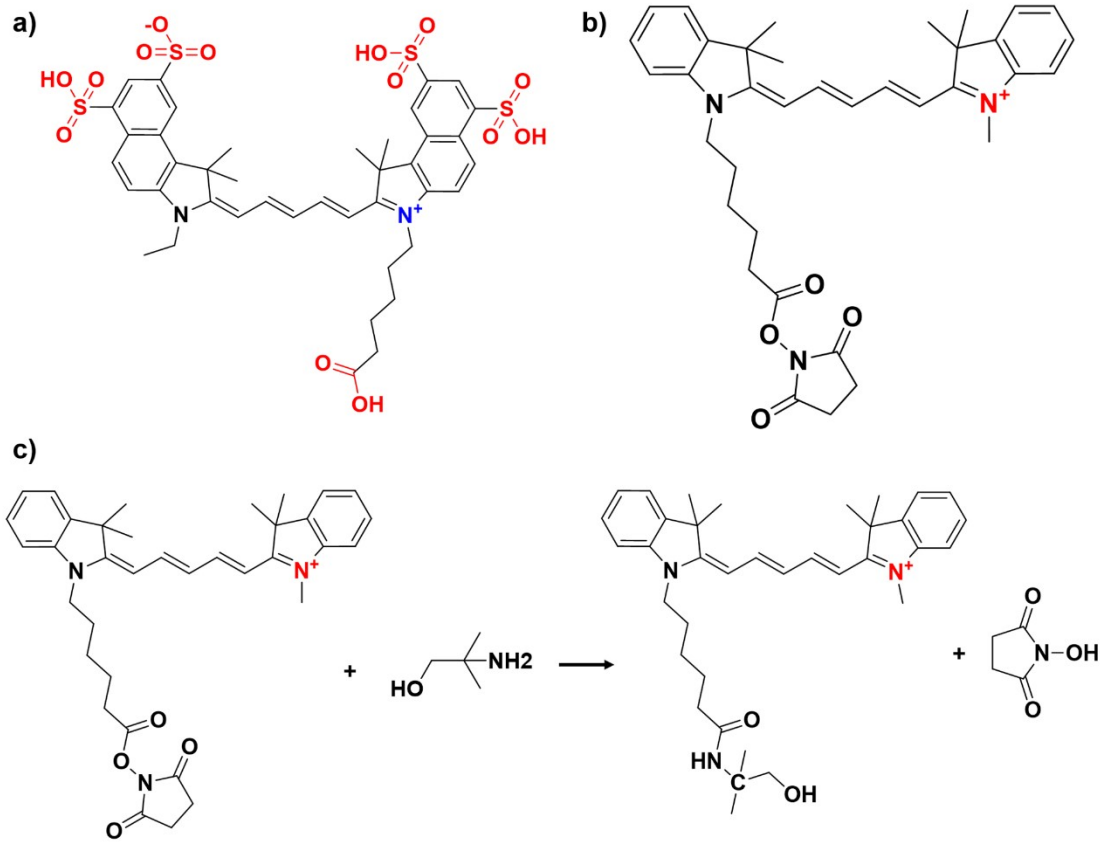

Figure S5. Structural formulae of (a) negatively charged Cy5.5, and (b) positively charged +Cy5. (c) Reaction of NHS group in the AMP electrolyte in positively charged fluorophore of +Cy5.

Figure S6. Statistics of the average collision numbers between fluorophores and water-air nanointerfaces on nanodroplets with different diameters

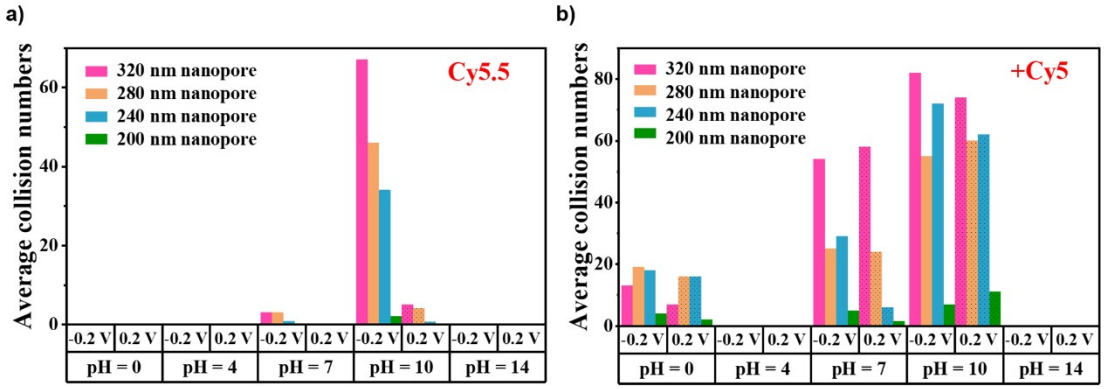

Figure S6. Statistics of the average collision numbers between fluorophores of (a) Cy5.5, (b) +Cy5 and the nanointerfaces on nanodroplets with different diameters under different pH environment at -0.2 V and 0.2 V.

Figure S7. HIM Characterization of Au nanoring electrode arrays containing nanopore arrays of different diameters

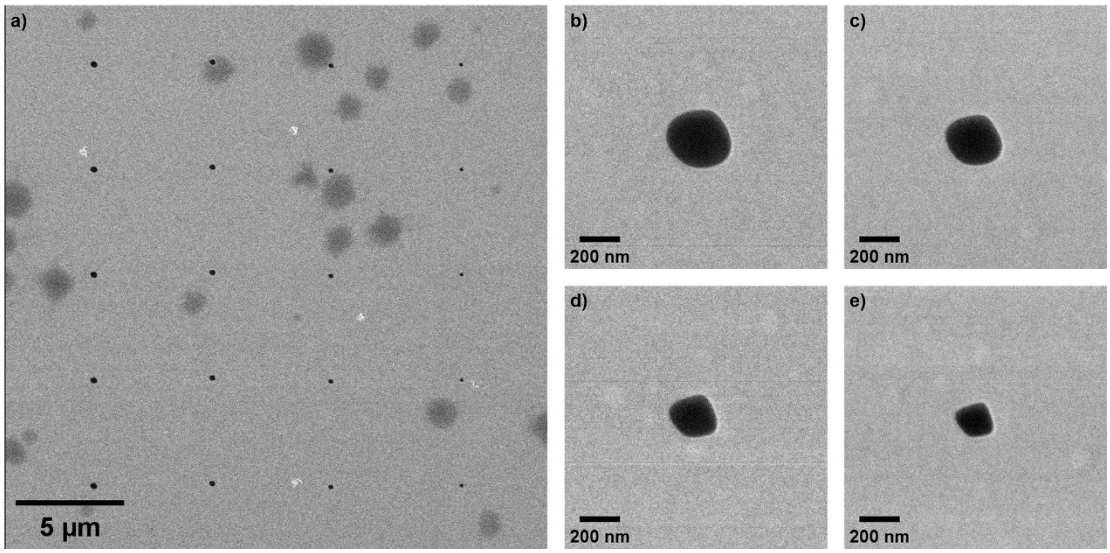

Figure S7. (a) HIM characterization results of the overall morphology of the Au nanoring electrode array. The Au nanoring electrode array consists of four 5 × 1 arrays of different diameters of 320 nm, 280 nm, 240 nm, and 200 nm from left to right. Detailed HIM morphology characterization results of the individual Au nanoring electrode arrays of (b) 320 nm, (c) 280 nm, (d) 240 nm, and (e) 200 nm contained in the array. HIM is imaged on the Au layer side of the Si chip.

Figure S8. Imaging of Cy5.5 in various pH environments at -0.2 V

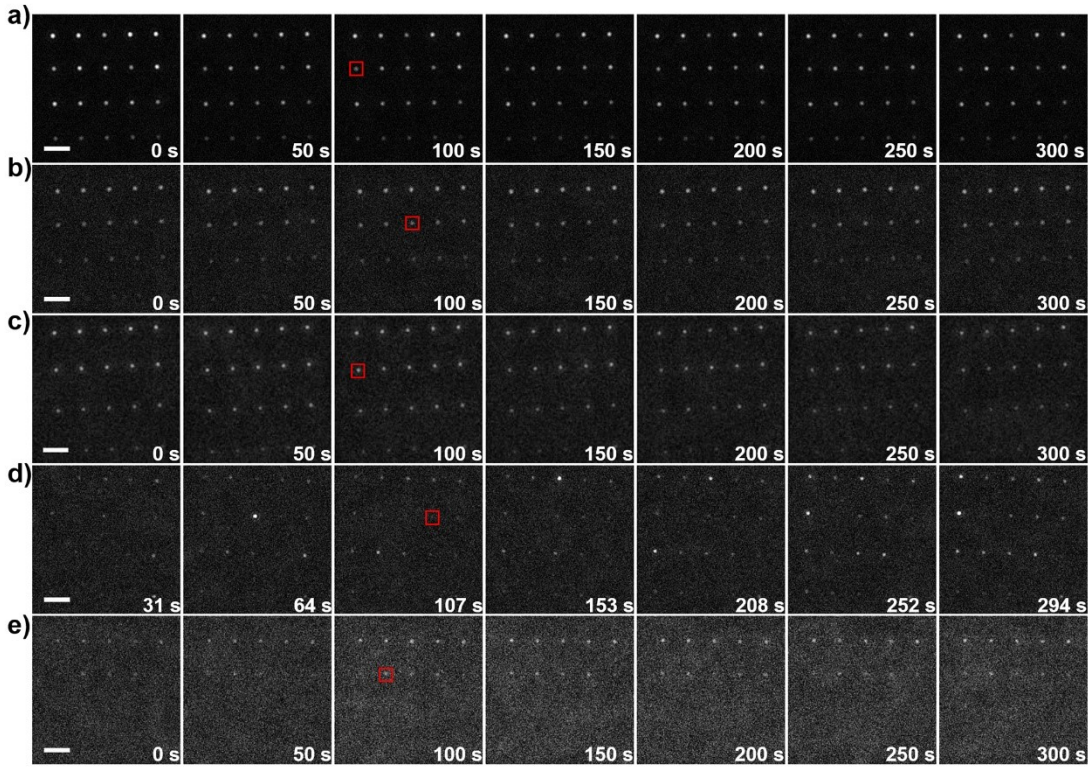

Figure S8. Imaging of Cy5.5 in (a) pH 0, (b) pH 4, (c) pH 7, (d) pH 10 and (e) pH 14 environments at -0.2 V, the scale bar is 5 μm. The fluorescence intensity change over time in Figure 2E were extracted from the nanodroplets marked in the red box. The Au nanoring electrode array consists of four 1 × 5 arrays of different diameters of 320 nm, 280nm, 240 nm, and 200 nm from top to bottom.

Figure S9. Imaging of Cy5.5 in various pH environments at 0.2 V

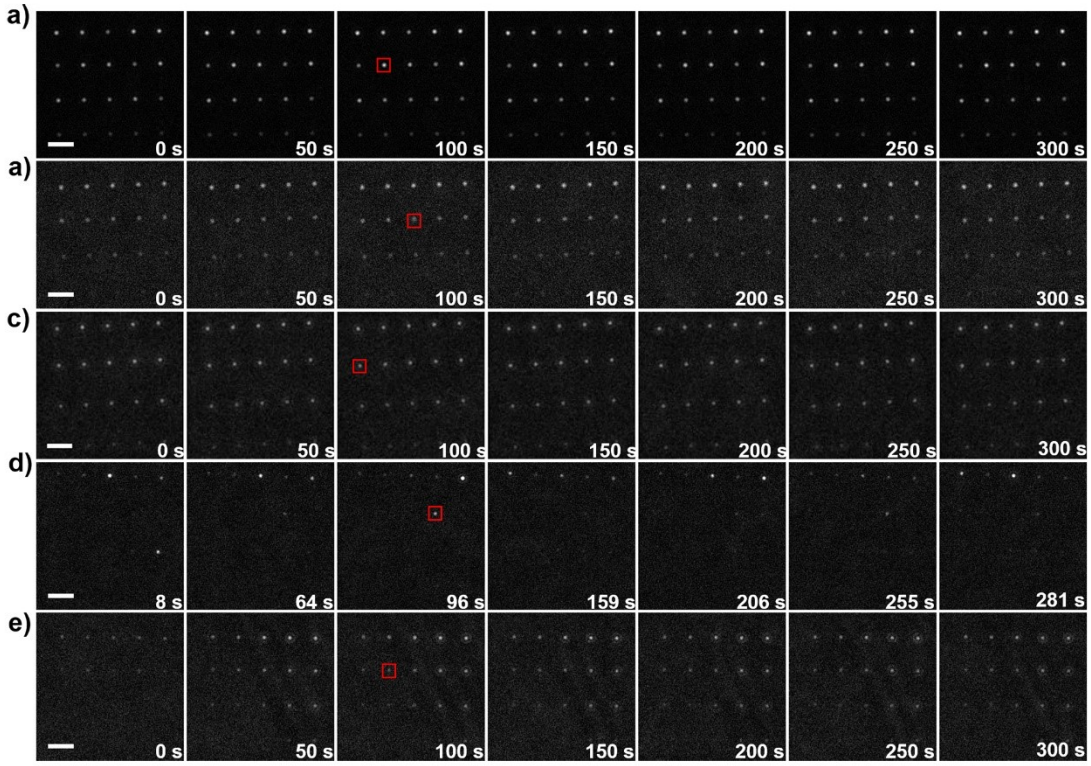

Figure S9. Imaging of Cy5.5 in (a) pH 0, (b) pH 4, (c) pH 7, (d) pH 10 and (e) pH 14 environments at 0.2 V, the scale bar is 5 μm. The fluorescence intensity change over time in Figure2F were extracted from the nanodroplets marked in the red box. The Au nanoring electrode array consists of four 1 × 5 arrays of different diameters of 320 nm, 280nm, 240 nm, and 200 nm from top to bottom.

Figure S10. Electrochemical curves of fluorescence response of Cy5.5 in different pH environments

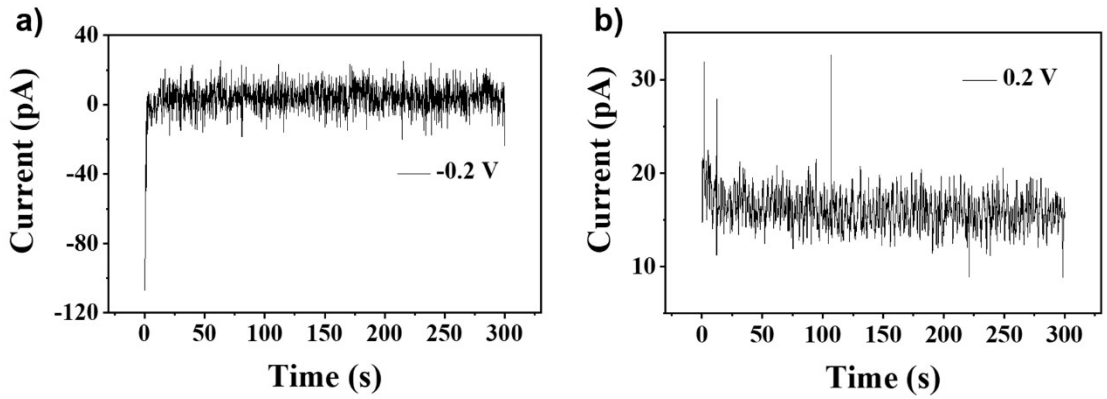

Figure S10. The most representative electrochemical curve at (a) -0.2 V corresponding to Figure S8 and (b) 0.2 V corresponding to Figure S9 for Cy5.5 under various pH environments.

Figure S11. Demonstration of three collision peaks with different durations at -0.2 V, pH 10 and no surfactant for Cy5.5

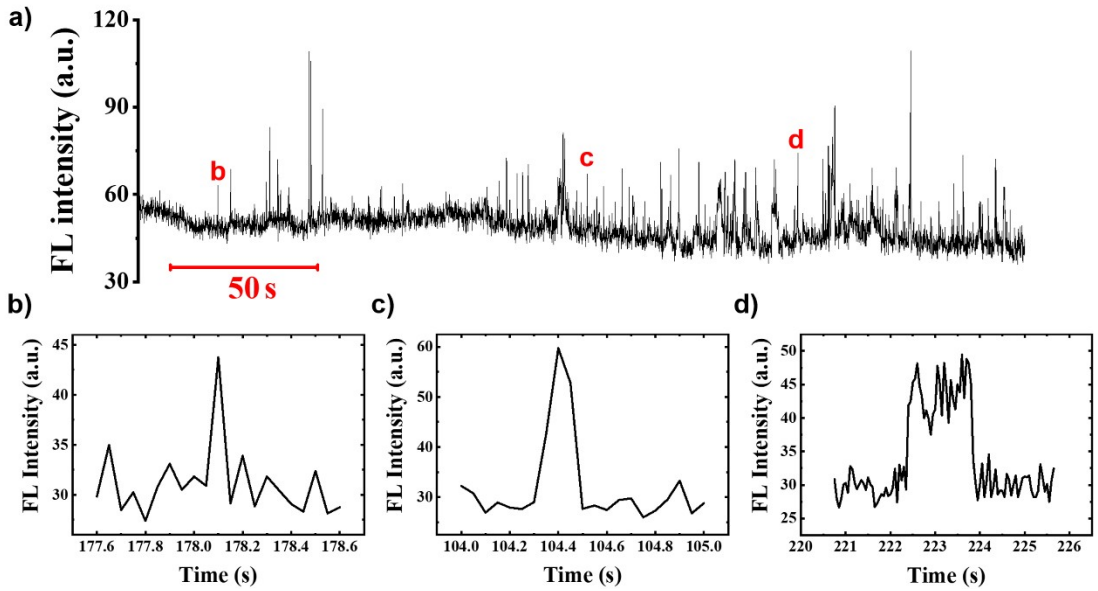

Figure S11: (a) Collision events of Cy5.5 with nanointerfaces at -0.2 V, pH 10 and no surfactant. Three collision peak types selected from Figure a with widths of (b) 50 ms, (c) 100-200 ms, and (d) wide (250 ms and above) respectively.

Figure S12. The statistical of collision numbers and peak relative height for Cy5.5 at -0.2 V, pH 10 and no surfactant

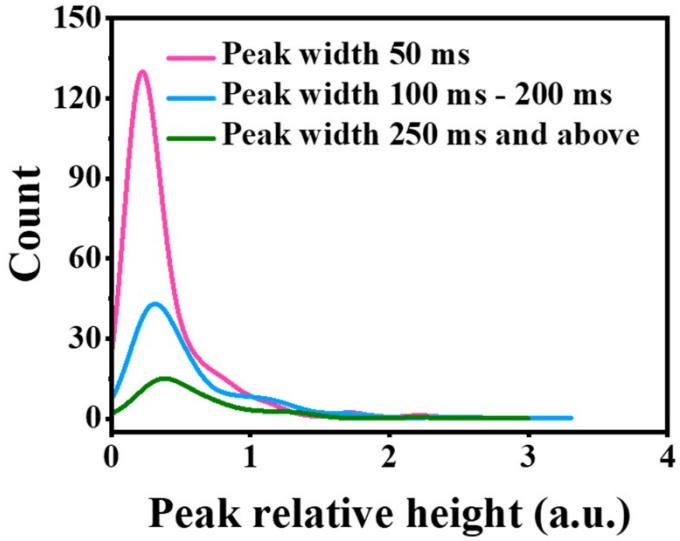

Figure S12: Statistics of the collision numbers counts with different peak widths versus the peak relative height for Cy5.5 at -0.2 V. pH 10 and no surfactant.

Figure S13. Imaging of +Cy5 in various pH environments at -0.2 V

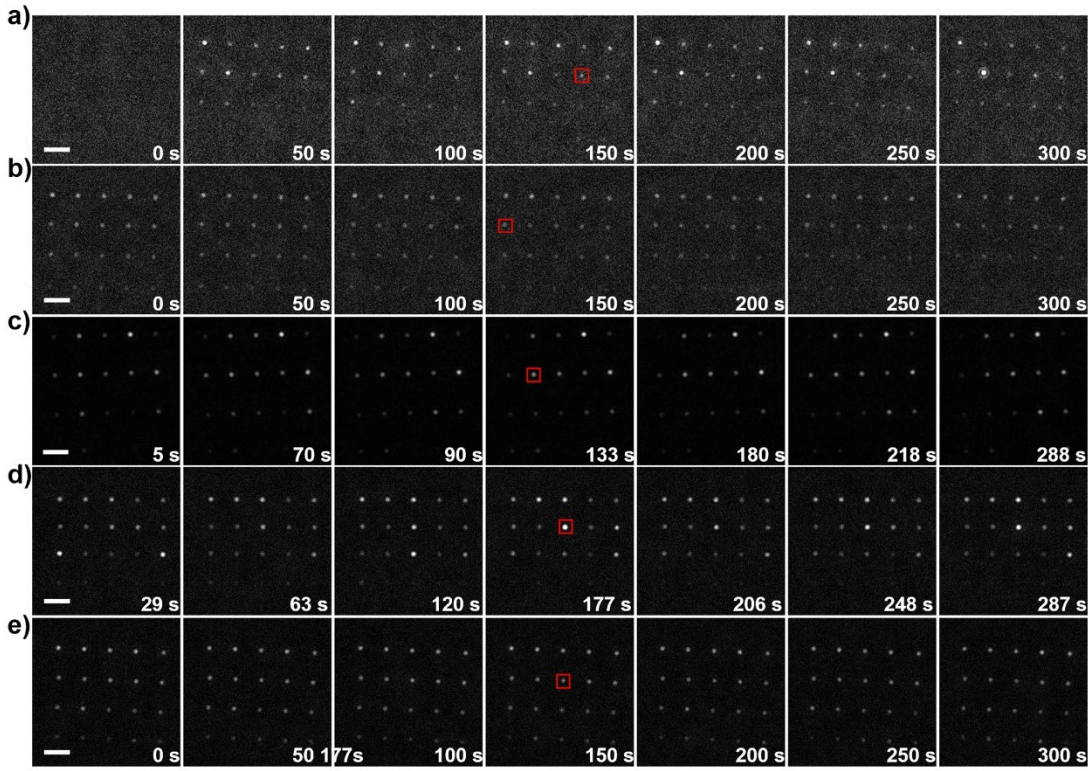

Figure S13. Imaging of +Cy5 in(a) pH 0, (b) pH 4, (c) pH 7, (d) pH 10 and (e) pH 14 environments at -0.2 V, the scale bar is 5 μm. The fluorescence intensity change over time in Figure 2G were extracted from the nanodroplets marked in the red box. The Au nanoring electrode array consists of four 1 × 5 arrays of different diameters of 320 nm, 280nm, 240 nm, and 200 nm from top to bottom.

Figure S14. Imaging of +Cy5 in various pH environments at -0.2 V

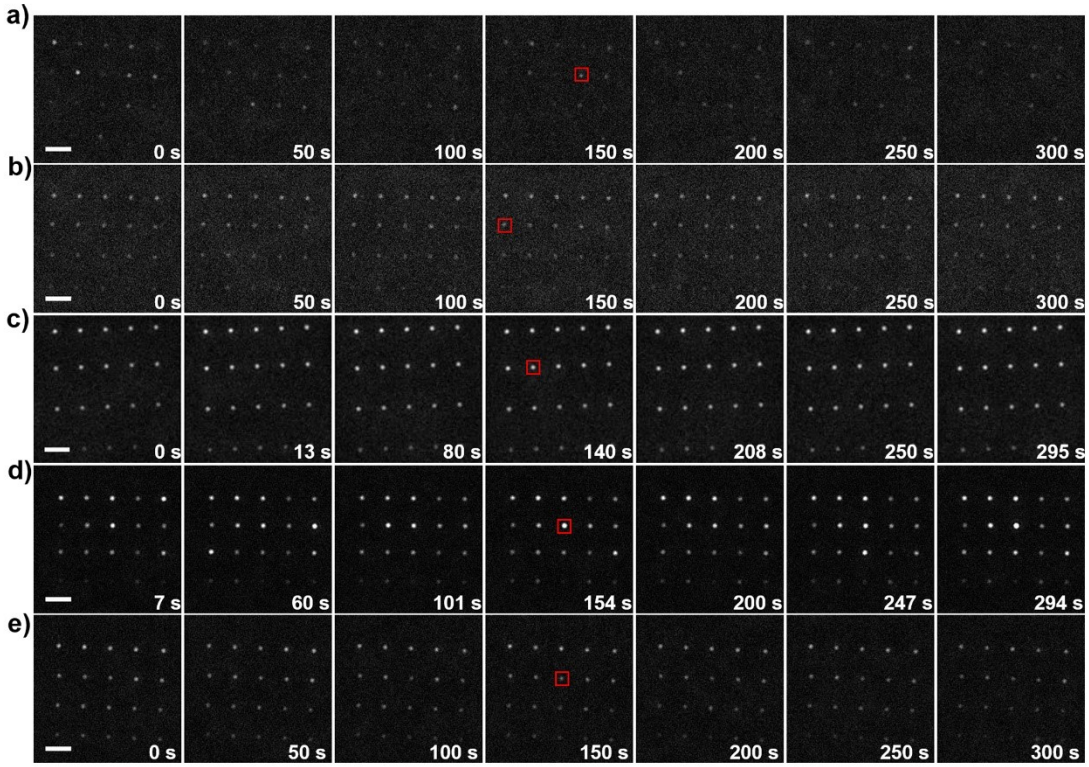

Figure S14. Imaging of +Cy5 in (a) pH 0, (b) pH 4, (c) pH 7, (d) pH 10 and (e) pH 14 environments at 0.2 V, the scale bar is 5 μm. The fluorescence intensity change over time in Figure 2H were extracted from the nanodroplets marked in the red box. The Au nanoring electrode array consists of four 1 × 5 arrays of different diameters of 320 nm, 280nm, 240 nm, and 200 nm from top to bottom.

Figure S15. Electrochemical curves of fluorescence response of +Cy5 in different pH environments

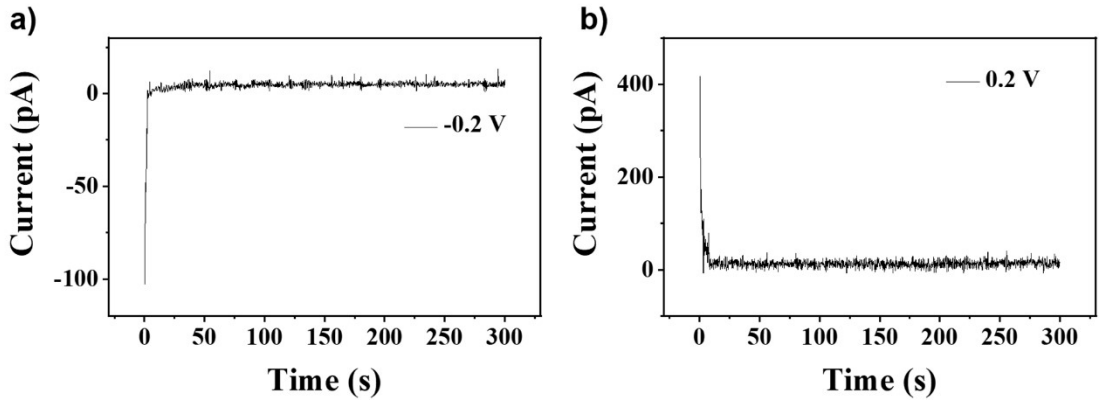

Figure S15. The most representative electrochemical curve at (a) -0.2 V corresponding to Figure S13 and (b) 0.2 V corresponding to Figure S14 for +Cy5 under various pH environments.

Figure S16. Effect of SDS on the curvature of the nanointerfaces while potential applied

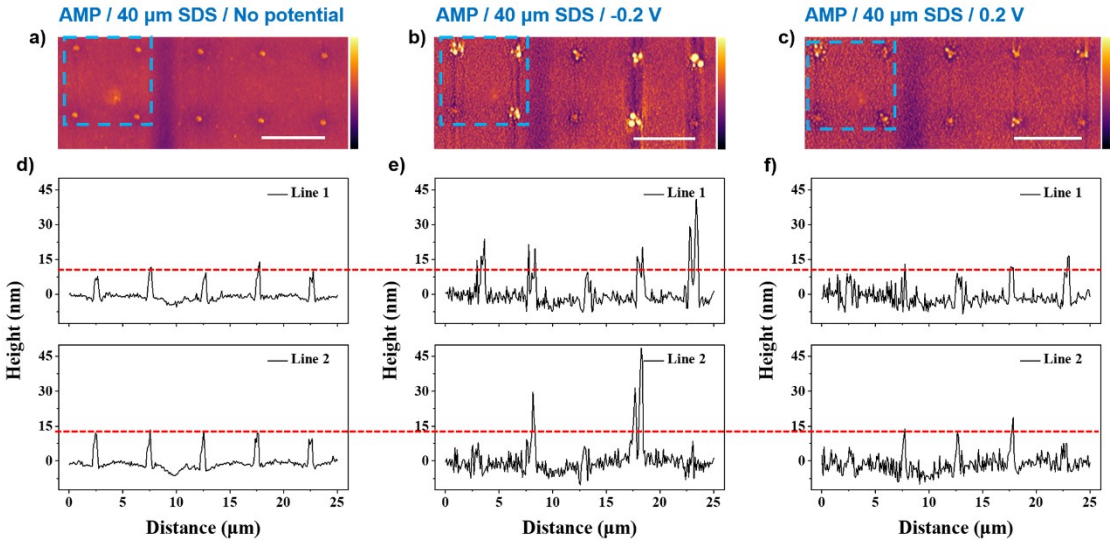

Figure S16. Detailed AFM characterization of nanointerfaces curvature in AMP electrolyte at (a) no potential, (b) -0.2 V, and (c) 0.2 V. Detailed height for AFM characterization in AMP electrolyte at (d) no potential, (e) -0.2 V, and (f) 0.2 V. The AMP buffers contains 40 μM SDS. The 2 × 2 array labeled by blue boxes are the results presented in Figures 3A-3C, respectively. The electrode array used here was a uniform 2 × 5 Au nanoring electrode array with an electrode diameter of 280 nm.

Figure S17. Effect of CTAB on the curvature of the nanointerfaces while potential applied

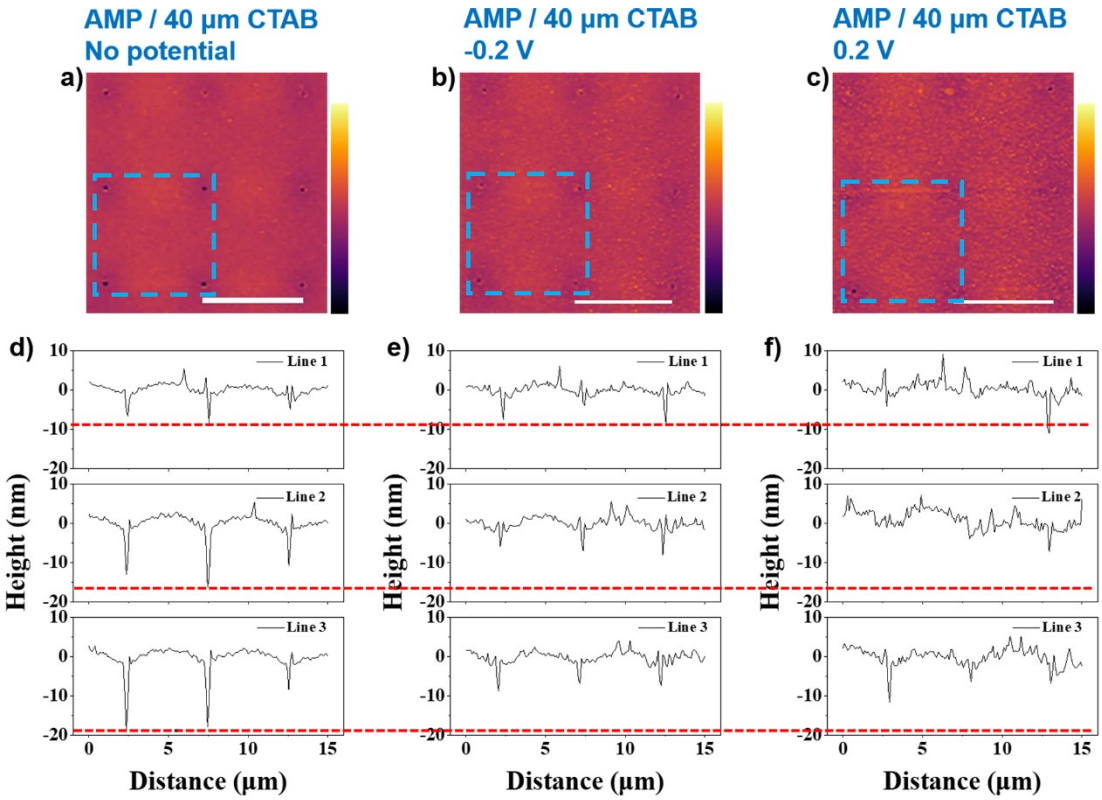

Figure S17. Detailed AFM characterization of nanointerfaces curvature in AMP electrolyte at (a) no potential, (b) -0.2 V, and (c) 0.2 V. Detailed height for AFM characterization in AMP electrolyte at (d) no potential, (e) -0.2 V, and (f) 0.2 V. The AMP buffers contains 40 μM CTAB. The 2 × 2 array labeled by blue boxes are the results presented in Figures 3F-3H, respectively. The electrode array used here was a uniform 3 × 3 Au nanoring electrode array with an electrode diameter of 280 nm.

Figure S18. Calibration of gold electrode

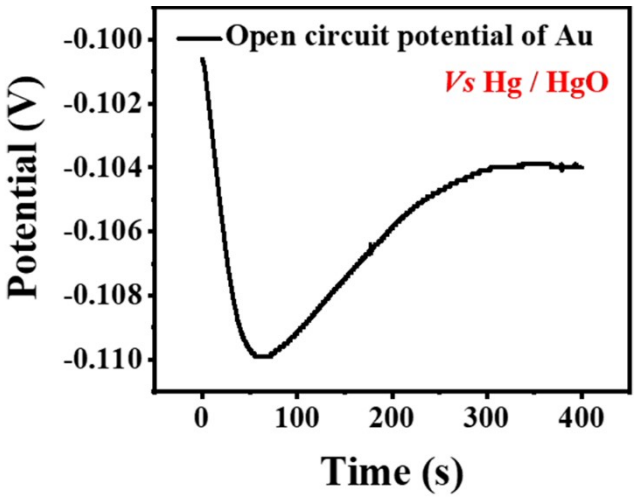

Figure S18. Calibration of gold electrode

As shown in Figure S16, the open-circuit potential of gold measured in AMP buffer with 40 μM CTAB was -0.104V (vs Hg / HgO). After calibration, the electrode potential of gold was 0.098 V - 0.104 V = -0.006 V (vs SHE). The standard electrode potential of Hg / HgO electrode is 0.098V.

Figure S19. Imaging of Cy5.5 in pH 10 AMP buffers containing different concentrations of SDS at -0.2 V

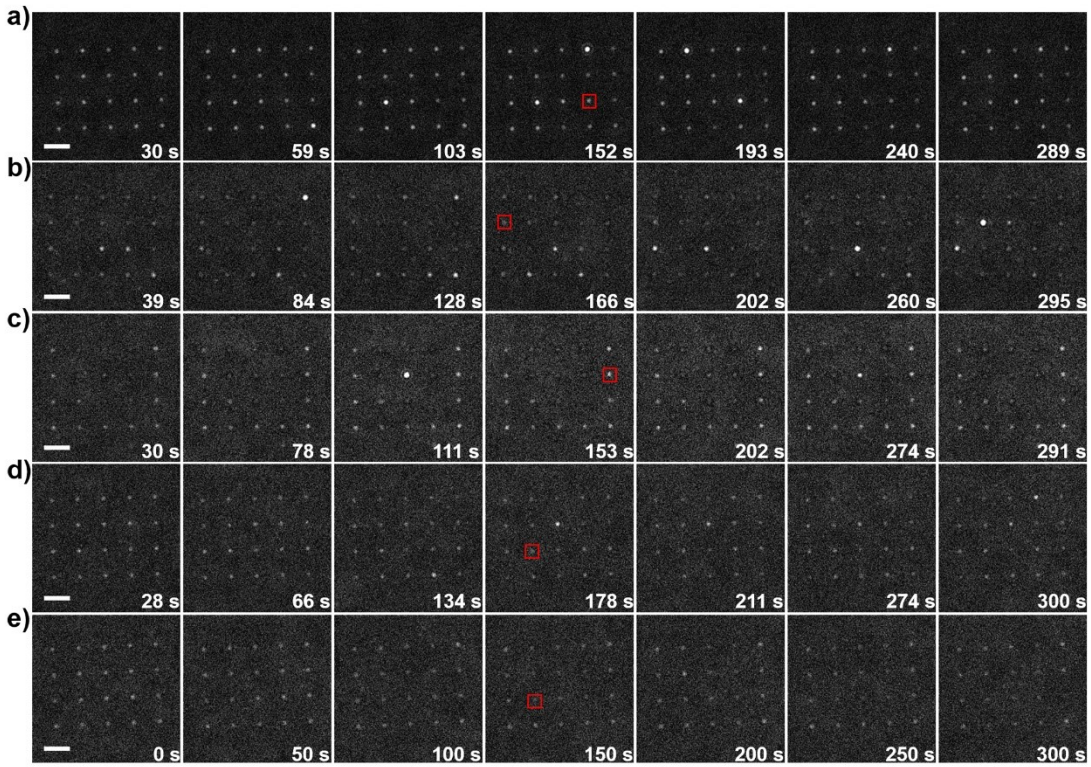

Figure S19. Imaging of Cy5.5 in pH 10 AMP buffers containing different concentrations of SDS at -0.2 V on a 4 × 5 uniform Au nanoring electrode array with an electrode diameter of 280 nm. (a) No SDS, (b) 20 μM SDS, (c) 40 μM SDS, (d) 60 μM SDS, and (e) 80 μM SDS. The scale bar is 5 μm. The curves of fluorescence intensity over time in Figure 4A were extracted from the nanodroplets labeled in the red box.

Figure S20. Imaging of Cy5.5 in pH 10 AMP buffers containing different concentrations of SDS at 0.2 V

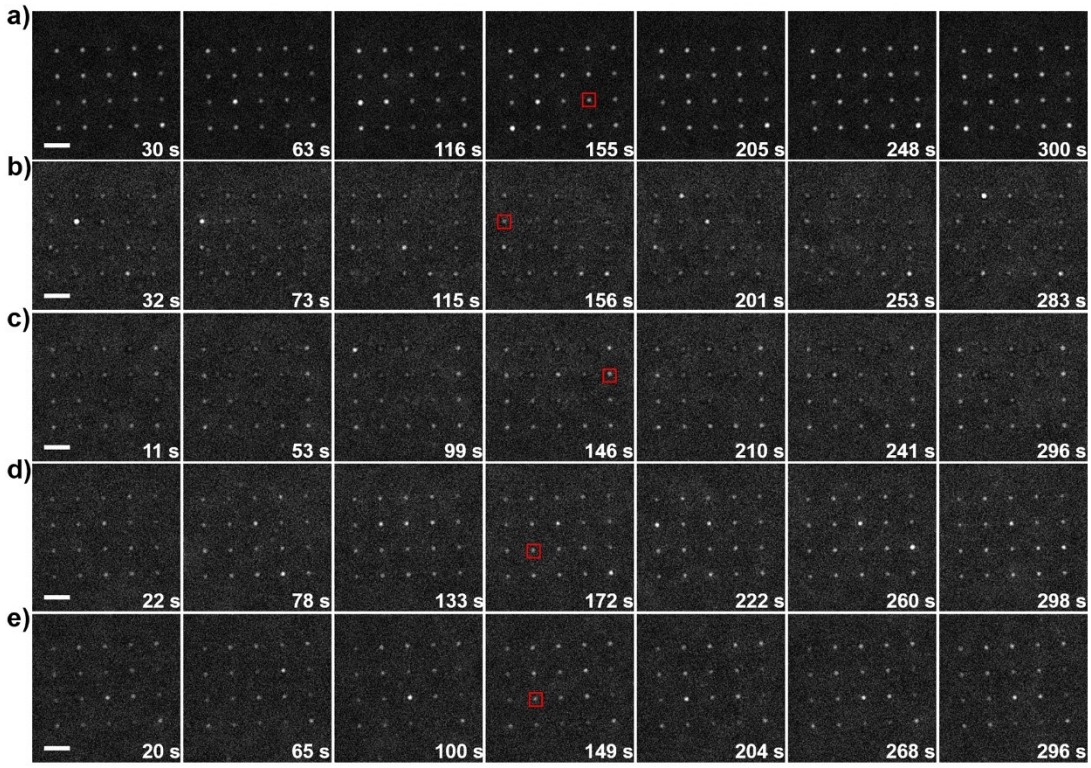

Figure S20. Imaging of Cy5.5 in pH 10 AMP buffers containing different concentrations of SDS at 0.2 V on a 4 × 5 uniform Au nanoring electrode array with an electrode diameter of 280 nm. (a) No SDS, (b) 20 μM SDS, (c) 40 μM SDS, (d) 60 μM SDS, and (e) 80 μM SDS. The scale bar is 5 μm. The curves of fluorescence intensity over time in Figure 4B were extracted from the nanodroplets labeled in the red box.

Figure S21. The most representative electrochemical curve at -0.2 V and 0.2 V for Cy5.5 under different concentrations of SDS at pH 10

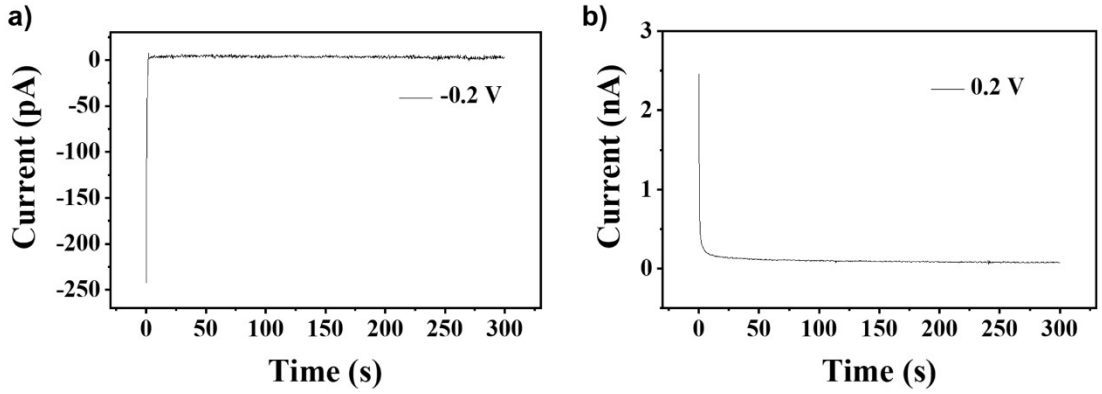

Figure S21. The most representative electrochemical curve at (a) -0.2 V corresponding to Figure S19 and (b) 0.2 V corresponding to Figure S20 for Cy5.5 under different concentrations of SDS at pH 10.

Figure S22. Imaging of Cy5.5 in pH 10 AMP buffers containing different concentrations of CTAB at -0.2 V

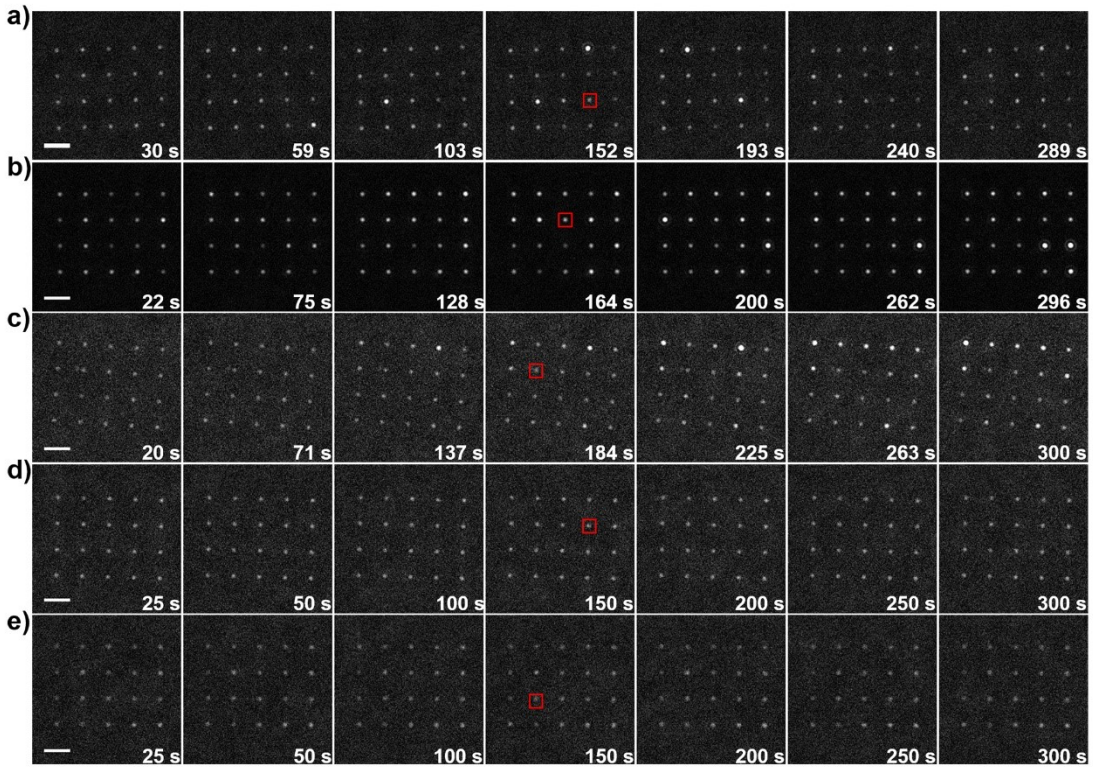

Figure S22. Imaging of Cy5.5 in pH 10 AMP buffers containing different concentrations of CTAB at -0.2 V on a 4 × 5 uniform Au nanoring electrode array with an electrode diameter of 280 nm. (a) No CTAB, (b) 20 μM CTAB, (c) 40 μM CTAB, (d) 60 μM CTAB, and (e) 80 μM CTAB. The scale bar is 5 μm. The curves of fluorescence intensity over time in Figure 4D were extracted from the nanodroplets labeled in the red box.

Figure S23. Imaging of Cy5.5 in pH 10 AMP buffers containing different concentrations of CTAB at 0.2 V

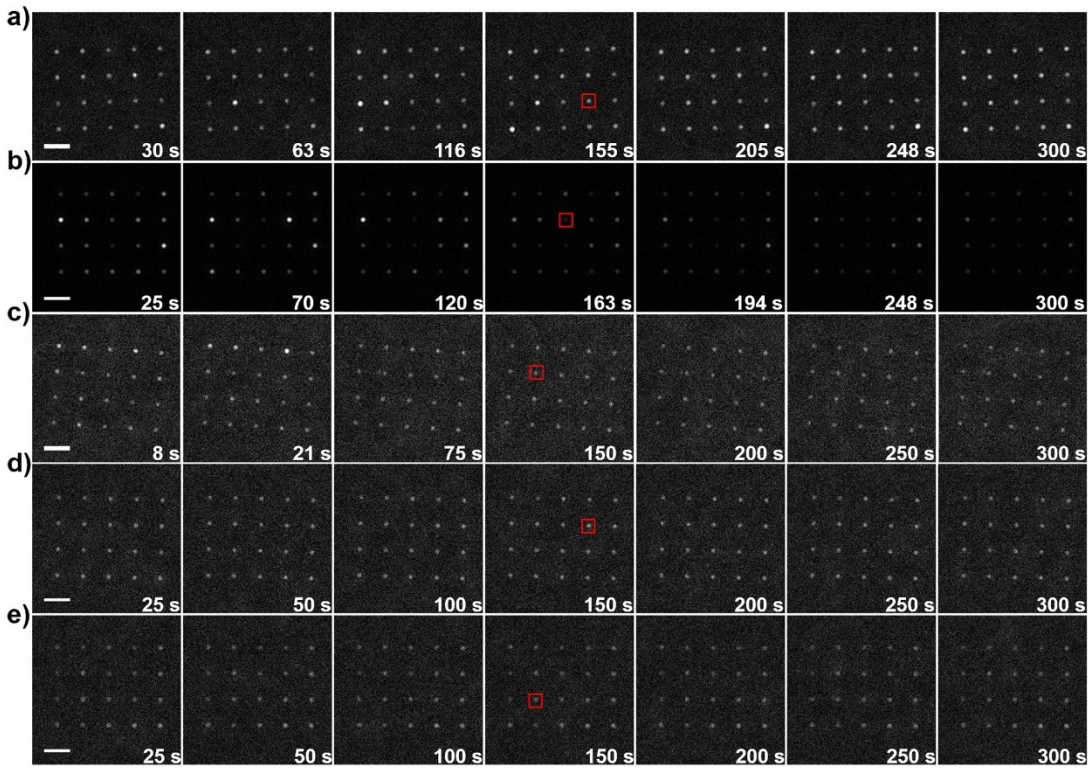

Figure S23. Imaging of Cy5.5 in pH 10 AMP buffers containing different concentrations of CTAB at 0.2 V on a 4 × 5 uniform Au nanoring electrode array with an electrode diameter of 280 nm. (a) No CTAB, (b) 20 μM CTAB, (c) 40 μM CTAB, (d) 60 μM CTAB, and (e) 80 μM CTAB. The scale bar is 5 μm. The curves of fluorescence intensity over time in Figure 4E were extracted from the nanodroplets labeled in the red box.

Figure S24. The most representative electrochemical curve at -0.2 V and 0.2 V for Cy5.5 under different concentrations of CTAB at pH 10

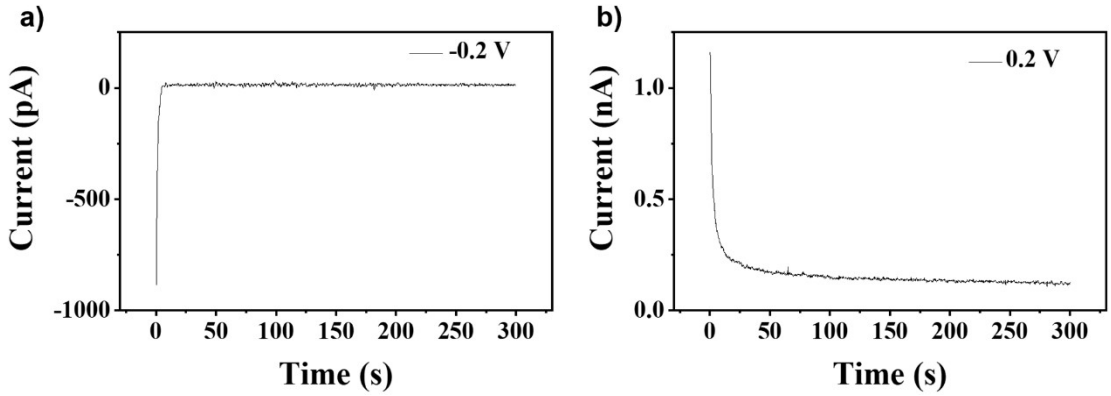

Figure S24. The most representative electrochemical curve at (a) -0.2 V corresponding to Figure S22 and (b) 0.2 V corresponding to Figure S23 for Cy5.5 under different concentrations of CTAB at pH 10.

Figure S25. Imaging of +Cy5 in pH 10 AMP buffers containing different concentrations of SDS at -0.2 V

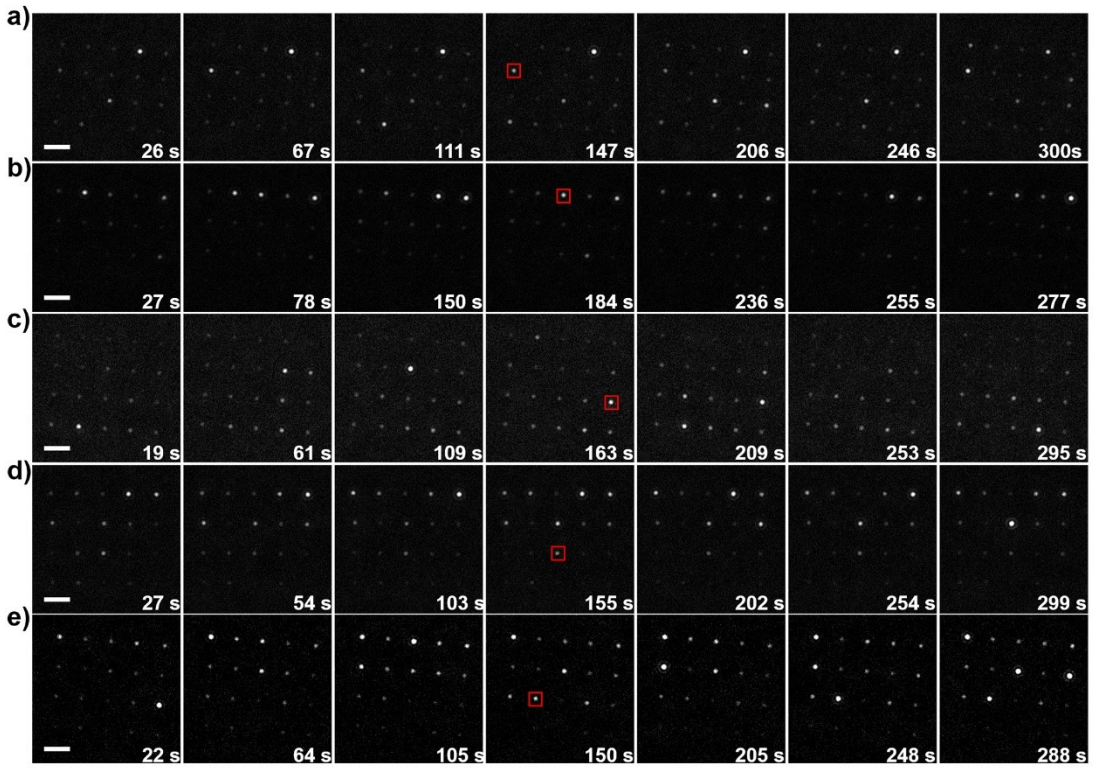

Figure S25. Imaging of +Cy5 in pH 10 AMP buffers containing different concentrations of SDS at -0.2 V on a 4 × 5 uniform Au nanoring electrode array with an electrode diameter of 280 nm. (a) No SDS, (b) 20 μM SDS, (c) 40 μM SDS, (d) 60 μM SDS, and (e) 80 μM SDS. The scale bar is 5 μm. The curves of fluorescence intensity over time in Figure 5A were extracted from the nanodroplets labeled in the red box.

Figure S26. Imaging of +Cy5 in pH 10 AMP buffers containing different concentrations of SDS at 0.2 V

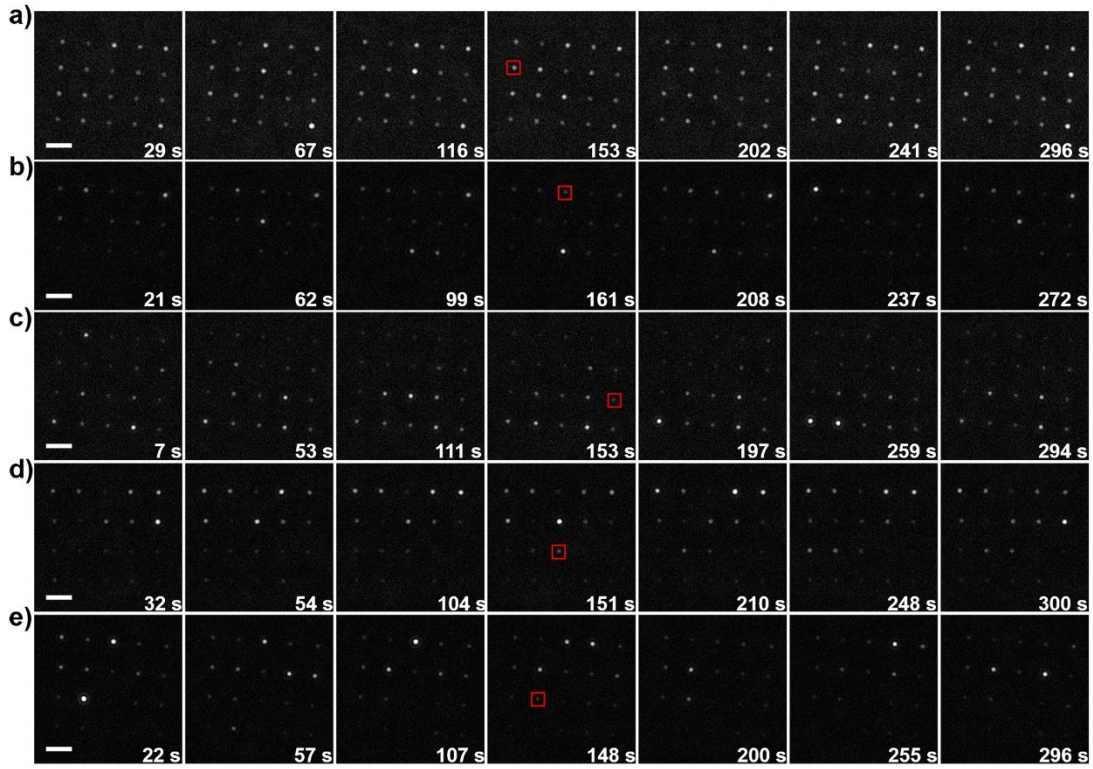

Figure S26. Imaging of +Cy5 in pH 10 AMP buffers containing different concentrations of SDS at 0.2 V on a 4 × 5 uniform Au nanoring electrode array with an electrode diameter of 280 nm. (a) No SDS, (b) 20 μM SDS, (c) 40 μM SDS, (d) 60 μM SDS, and (e) 80 μM SDS. The scale bar is 5 μm. The curves of fluorescence intensity over time in Figure 5B were extracted from the nanodroplets labeled in the red box.

Figure S27. The most representative electrochemical curve at -0.2 V and 0.2 V for +Cy5 under different concentrations of SDS at pH 10

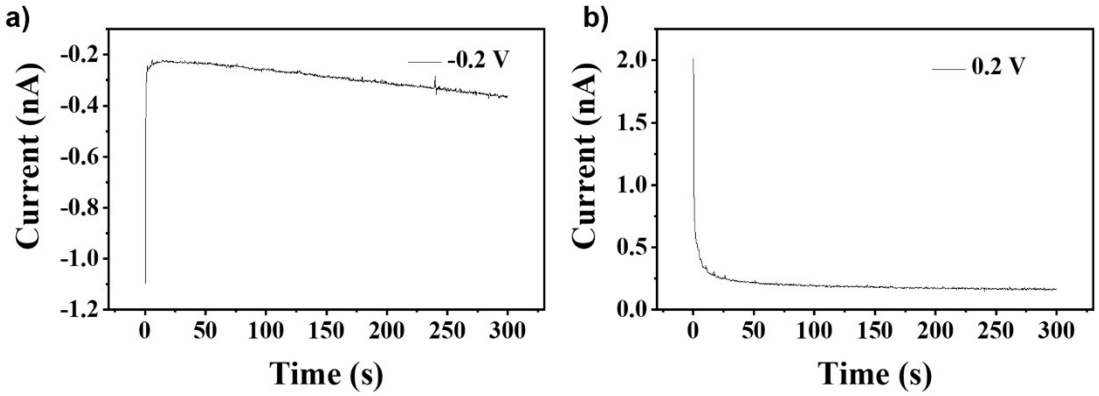

Figure S27. The most representative electrochemical curve at (a) -0.2 V corresponding to Figure S25 and (b) 0.2 V corresponding to Figure S26 for +Cy5 under different concentrations of SDS at pH 10.

Figure S28. Imaging of +Cy5 in pH 10 AMP buffers containing different concentrations of CTAB at -0.2 V

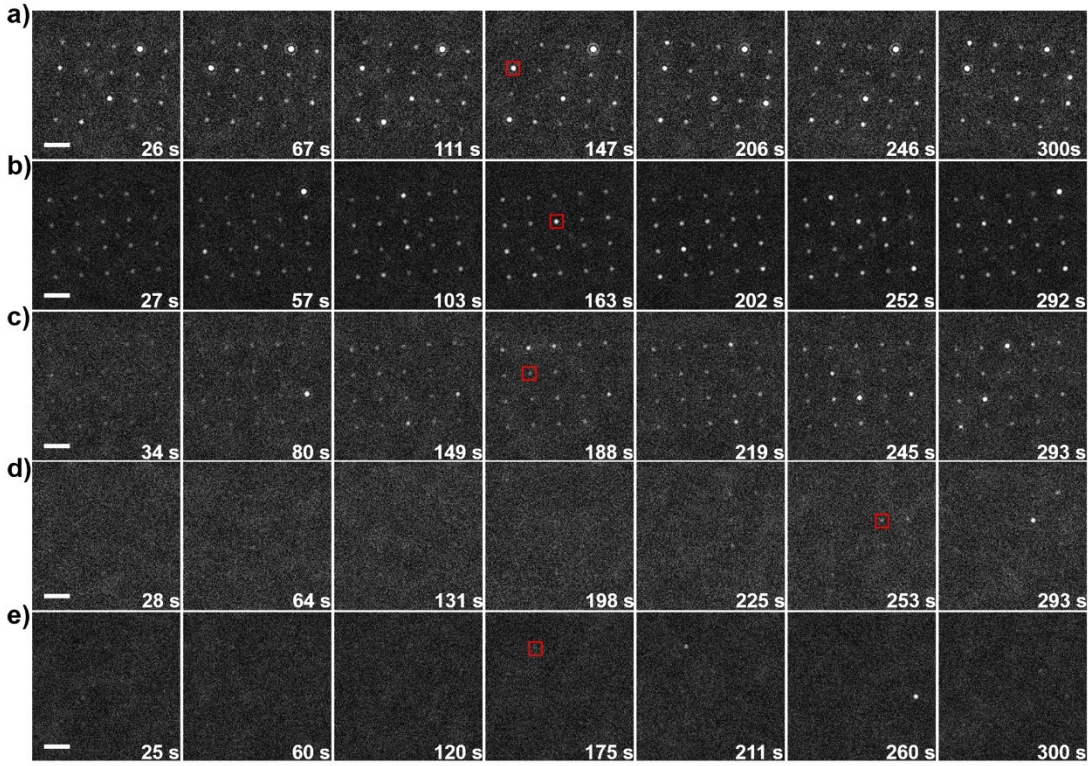

Figure S28. Imaging of +Cy5 in pH 10 AMP buffers containing different concentrations of CTAB at -0.2 V on a 4 × 5 uniform Au nanoring electrode array with an electrode diameter of 280 nm. (a) No CTAB, (b) 20 μM CTAB, (c) 40 μM CTAB, (d) 60 μM CTAB, and (e) 80 μM CTAB. The scale bar is 5 μm. The curves of fluorescence intensity over time in Figure 5D were extracted from the nanodroplets labeled in the red box.

Figure S29. Imaging of +Cy5 in pH 10 AMP buffers containing different concentrations of CTAB at 0.2 V

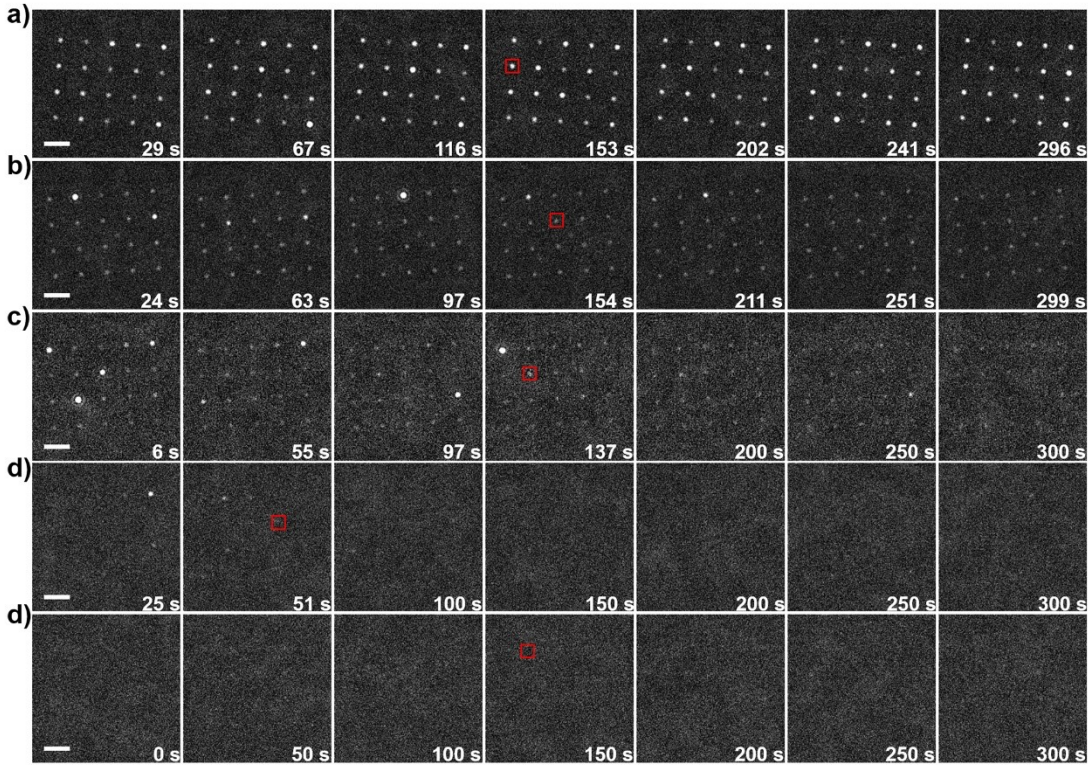

Figure S29. Imaging of +Cy5 in pH 10 AMP buffers containing different concentrations of CTAB at 0.2 V on a 4 × 5 uniform Au nanoring electrode array with an electrode diameter of 280 nm. (a) No CTAB, (b) 20 μM CTAB, (c) 40 μM CTAB, (d) 60 μM CTAB, and (e) 80 μM CTAB. The scale bar is 5 μm. The curves of fluorescence intensity over time in Figure 5E were extracted from the nanodroplets labeled in the red box.

Figure S30. The most representative electrochemical curve at -0.2 V and 0.2 V for +Cy5 under different concentrations of CTAB at pH 10

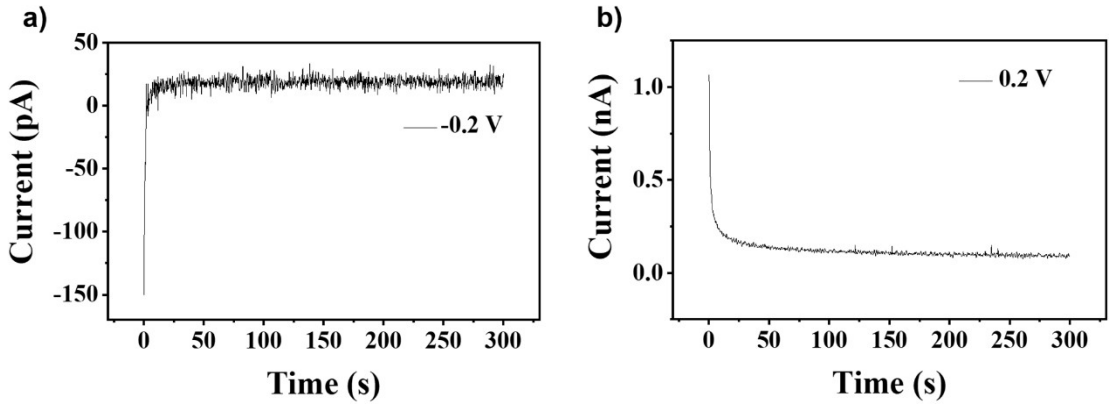

Figure S30. The most representative electrochemical curve at (a) -0.2 V corresponding to Figure S28 and (b) 0.2 V corresponding to Figure S29 for +Cy5 under different concentrations of CTAB at pH 10.

Figure S31. Fabrication of Au nanoring electrode array

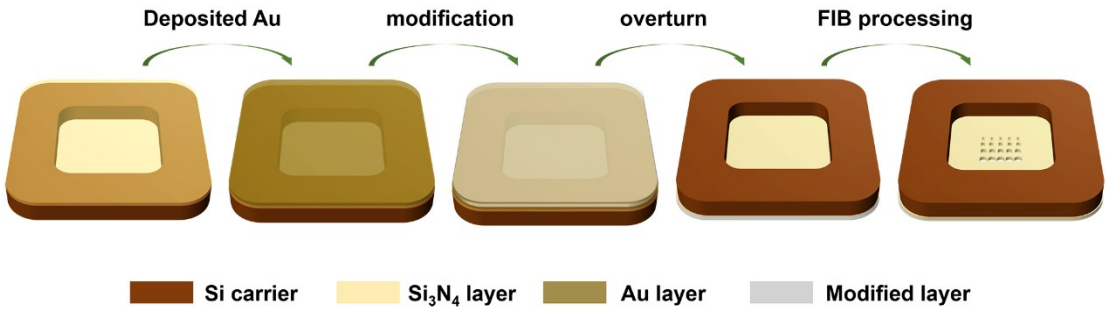

Figure S31. Schematic diagram of fabrication process of Au nanoring electrode array

Figure S32. Nanodroplet electrochemical cell

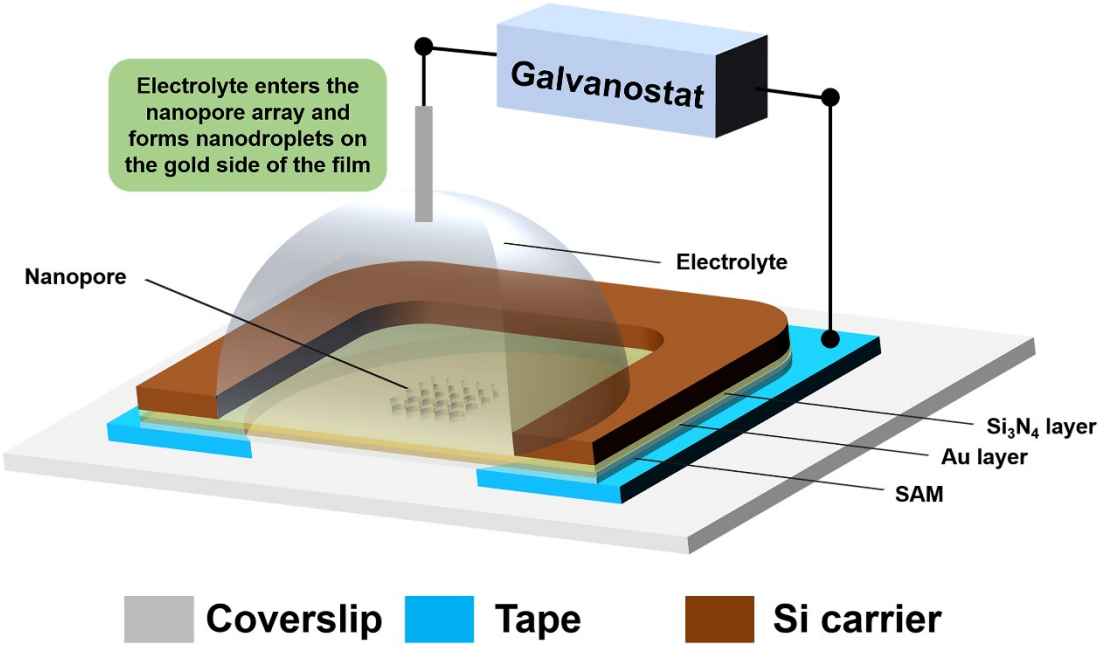

Figure S32. Structure diagram of nanodroplet electrochemical cell

Figure S33. Optical imaging setup

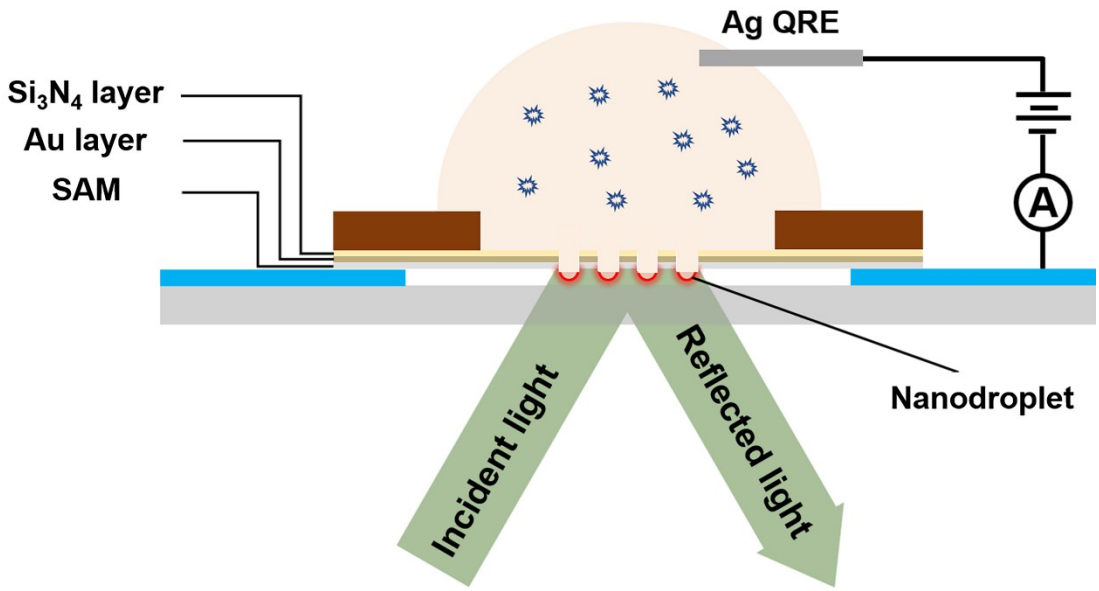

Figure S33. Structure diagram of the optical device imaging a nanodroplet electrochemical cell.